Diffusion-based design of locally resonant sub-systems using a reduced wave finite element framework

Christophe Droz, R Boukadia, M Ichchou, W Desmet

Diffusion-based design of locally resonant sub-systems using a reduced wave finite element framework

C. Droz [1], **R. Boukadia** [1], **M. Ichchou** [2], **W. Desmet** [1]
[1] Noise and Vibration Research Group, PMA Division, KU Leuven, Belgium

[2] Vibroacoustics and Complex Media Research Group, LTDS, Ecole Centrale de Lyon, France

Abstract
This paper presents a diffusion formulation for the Wave Finite Element (WFE) Framework, applied to the design of micro-resonators for low-frequency vibration control. First, the information resulting from diffusion analysis is compared with the one provided by a direct application of Bloch theory, in the case of periodically distributed resonators. Main advantages of diffusion methods are that the spacing between the resonators can be modified without resuming unit-cell analysis and that scattering effects, inherently produced by the host structure, can be distinguished from the sole resonator's influence. Then, the method is combined with an existing wave-based state vector reduction scheme to further reduce the computational efforts. Formulation is introduced and applied to a rectangular host structure with 3D-modeled resonators bonded on its surface. Eventually, damping-related transmission, reflection and diffusion effects produced by the resonators are studied around their harmonic frequency.

1 Introduction

Locally resonant materials have been widely studied over the past years especially in transportation and aerospace industry, where vibroacoustic requirements are increasingly demanding. A broad range of low- or mid-frequency phenomena can occur in these structures, which can be exploited to enhance their dynamic or acoustic responses. Innovative lightweight meta-structures with incorporated vibration control systems can therefore be engineered to enhance broadband vibroacoustic performances. The concept of tuned mass damping (or harmonic oscillators) can be implemented at the material's scale to achieve vibration control, often using periodically distributed resonators [1, 2].

In periodic waveguides, we distinguish Bragg-type bandgaps from local resonance (LR) effects: the first is ruled by the ratio between the periodic unit-cell dimension and the wavelength of propagating waves. The second is produced by internal resonances and depends on the waveguide's unit-cell inner dynamics. In this case, resonators can be artificially distributed to produce LR bandgaps without altering the host structure. Bloch theory is often used in this case to design and tune the resonators so that certain modes can be suppressed from the overall structure in the selected bandwidth [3, 4]. It is evident that such LR can be obtained without requiring a periodic distribution pattern, as in vibration control strategies based on multiple tuned mass dampers (TMD). Therefore, the use of Bloch/unit-cell modeling methods has two weaknesses: 1) it is based on a perfect periodicity assumption and yields often undesired Bragg-type dispersion effects, and 2) the modeling and computational effort being related to the dimensions of the unit-cell, it increases with the spacing between resonators.

An alternative modelling strategy is proposed in this paper, based on the wave diffusion properties of the harmonic oscillator. In this context, 'diffusion' refers to an elastic wave's reflection, transmission, and absorption process, as well as its specular and diffuse scattering analogues. In the Wave Finite Element Framework, the diffusion coefficients were first used by Mencik and Ichchou [5] to establish the junction between

two waveguides. Applications were proposed for wave scattering analyses with angular incidence [6], pipes [7, 8], curved periodic waveguides (see Errico et al. [9, 10]) and to evaluate the scattering effects through a variety of waveguides' junctions [11]. Wave diffusion analyses were also used to perform damage inspection in composite panels [12]. Recent studies addressed the coupling between electro-mechanical waveguides (see Lousoan et al. [13]).

Yet, these methods have failed so far to address large-scaled realistic structures, mainly due to the ill-conditioned nature of the scattering problem. The above-mentioned can thus be limited to small-scaled waveguides, or neglect decaying or evanescent waves. In this work a well-conditioned formulation is proposed and combined with a reduced-order modeling strategy [14] to perform fast diffusion analyses in a 3D modeled resonator bonded on a host structure and investigate the reflected, transmitted and diffusely scattered waves produced around the resonance frequency.

2 Periodic locally resonant system design

2.1 Bloch-based design

Consider a waveguide consisting of a host structure with periodically distributed resonators bonded on its surface. Bloch-based design can be achieved by considering a periodic unit-cell whose length depends on the spacing d between resonators. Then, denoting $\mathbb{K}$, $\mathbb{C}$ and $\mathbb{M}$ the finite element stiffness, damping and mass matrices of the periodic waveguide's unit-cell, the wave dispersion characteristics can be computed by solving the inverse Bloch problem Eq.(1):

$$[\mathbb{K}(\Delta) + j\omega\mathbb{C}(\Delta) - \omega^2\mathbb{M}(\Delta)]\Phi = 0 \tag{1}$$

where Δ is the propagation constant matrix and Φ is the wave solution.

For frequency-dependent problems such as diffusion or forced response analyses, one can solve the Direct Bloch problem Eq.(2) instead:

$$[\mathbb{D}_{RL}(\omega)\Delta^{-1} + (\mathbb{D}_{RR}(\omega) + \mathbb{D}_{LL}(\omega)) + \mathbb{D}_{LR}(\omega)\Delta]\Phi = 0 \tag{2}$$

where the dynamic stiffness sub-matrix is denoted $\mathbb{D}_{ab}(\omega) = \mathbb{K} + j\omega\mathbb{C} - \omega^2\mathbb{M}$ with a and b stand for left or right sides. Dynamic condensation is usually performed on matrix $\mathbb{D}$, and Component Mode Synthesis is generally used to increase computation efficiency.

The resolution of Eq.(2) provides a set of eigenvalues and vectors (wave shapes) describing the free wave propagation characteristics in the infinite waveguide. The propagation constants $\Delta = \{\lambda_i\}$ relate the displacements between two consecutive unit-cells and can be used to distinguish positive, negative, propagating and evanescent waves. For positive-going waves, the bandgap phenomenon is associated with a reduction of the propagation constant's norm $|\lambda|$ between 1 (propagating) and 0 (evanescent). It should be reminded that this indicator does not reflects a local attenuation ratio, but is related to the unit-cell's scale. An equivalent spatial attenuation in dB per unit-length can be derived using the complex wavenumber $k = \Re(k) + j\Im(k)$ definition: $\lambda = \exp(-jkd)$, which provides a simple estimation of the classical spatial attenuation indicator α:

$$\alpha(dB/m) = 10\frac{\log_{10}\left(|\frac{u_{n+1}}{u_n}|^2\right)}{d} \tag{3}$$

The expression Eq.4 can be approximated into:

$$\alpha(dB/m) \approx 8.686 \times \Im(k) \tag{4}$$

The value of α can be chosen instead of $|\lambda|$ to evaluate the attenuation performances of the periodic waveguide. For Direct Bloch resolution, a wave matching algorithm is then used to track flexural wave's frequency dependent solutions inside the bandgap.

2.2 FE Modeling and materials

The host structure is a thin rectangular beam of dimensions 3 cm $\times$ 1.1 m. The resonators are made of a 3D printed polymer. Material and damping properties used in the FE model are described in Table 1. The influence of the resonator's damping properties will be further investigated in sec.4.3.

Part-Component	Density ρ	Young Modulus E	Shear mod. G	Loss factor η (%)
Host	2700	70×10^9	26.3×10^9	0.2
Resonator	1400	1.8×10^9	0.54×10^9	5
Mass	2700	70×10^9	26.3×10^9	0.2

Table 1: Material properties of the waveguide and resonator models.

A parametric model of the periodic unit-cell is shown in Fig. 1 and numerical applications are based on the dimensions of table 2. The length l_0 represents the spacing between the resonators. The resonator is centered on the waveguide unit-cell in the y-direction and can be placed arbitrarily along the x-direction as it remains periodic. The unit-cell is converged and meshed using linear elements and a total of 5500 DOFs.

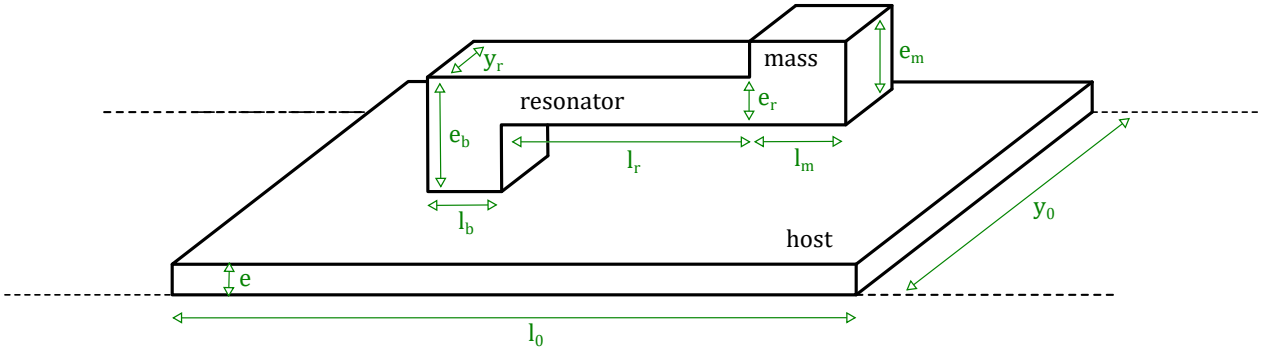

Figure 1: Description of the periodic unit-cell use for Bloch analyses.

Parameter	value (mm)	Parameter	value (mm)
l_0	55	e	2.5
y_0	30	y_r	15
l_b	10	e_b	9
l_r	30	e_r	3
l_m	10	h_m	13

Table 2: Geometric model of the tuned mass damper and periodic unit-cell description.

2.3 Interpretation of the band diagram

Dispersion diagram shown in Fig.2.a is computed using periodic Bloch model for the unit-cell described above. The first local resonance is identified at 339 Hz, corresponding to the bending mode of the tuned mass damper. Bandgap is observed for the transverse vertical (flexural) wave, while the shear, torsional and longitudinal waves are not affected by the resonator. The wave attenuation $\Im(k)$ is presented on the colormap while the propagation constant norm $|\lambda|$ is plotted in Fig. 2.b. Both indicating a drastic attenuation between 320 Hz and 360 Hz.

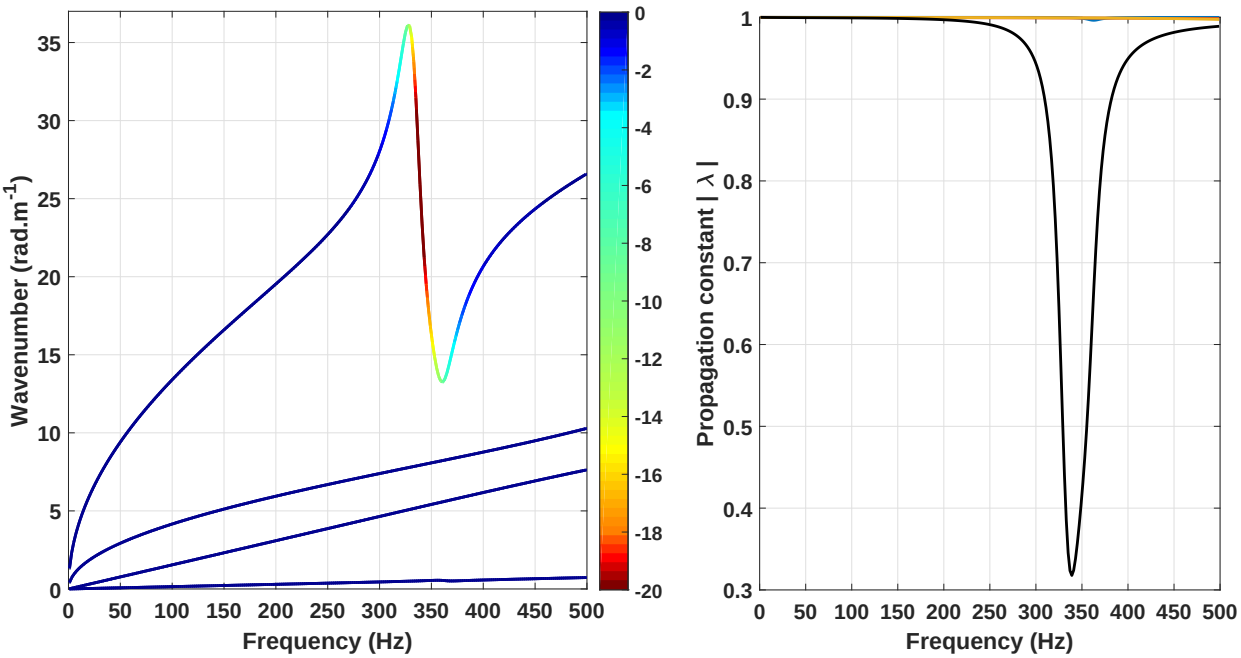

Figure 2: Dispersion diagram calculated using Bloch theory on periodic unit-cell model. (a) Wavenumber (real and imaginary). (b) Norm of the complex propagation constant.

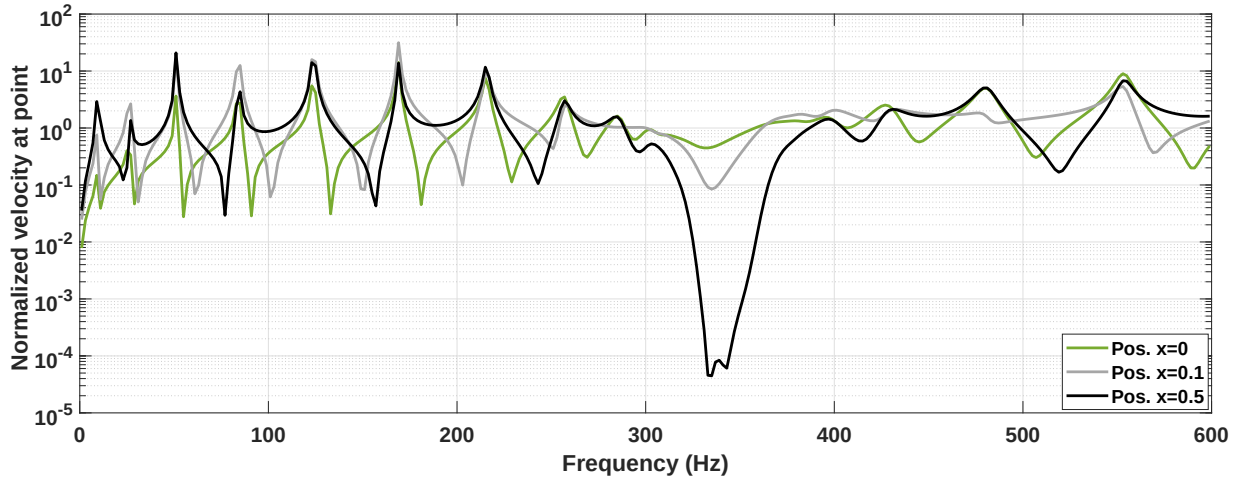

Figure 3: FRF of the free-clamped waveguide to point force excitation at the free end. Three positions from excitation point (0 cm, 10 cm, 50 cm).

The dispersion results are compared with the finite waveguide's dynamic response in Fig. 3. Clamped-free boundary conditions are considered and a point force excitation is applied at a free end. Normal velocities are plotted at three distances: 0 cm, 10 cm and 50 cm from the excitation point, corresponding to 0, 1 and 9 resonators, respectfully. Dynamic modes are clearly suppressed in the resonance bandwidth and strongly damped from 300 Hz to 400 Hz.

Far for the source excitation, the dynamic response exhibits a gap well predicted by the propagation constant, while in the near-field the presence of the resonators only suppresses the waveguide's modes. We can conclude from these results that the propagation constants provided by Bloch-based analyses are an efficient

way to design a network of periodically distributed tuned mass dampers. However, it is emphasized that the value of $|\lambda|$ only stands for the wave transmitted amplitude, but does not distinguishes internal dissipation, diffusion nor reflection, which produce different vibration attenuation.

3 Waveguide Diffusion Modeling

3.1 Concept

The proposed modeling strategy consists in replacing the locally resonant unit-cell by two semi-infinite waveguides connected using a small section of the waveguide supporting the resonator. Therefore, Bloch theory is no longer applied to the global unit-cell as above, but on the elementary waveguide's cross-section, involving only 312 DOFs. Wave solutions will be denoted (Λ, Ψ) for this base waveguide's solutions, instead of (Δ, Φ) for the global periodic unit-cell. The diffusion-based model is illustrated in Fig. 4.

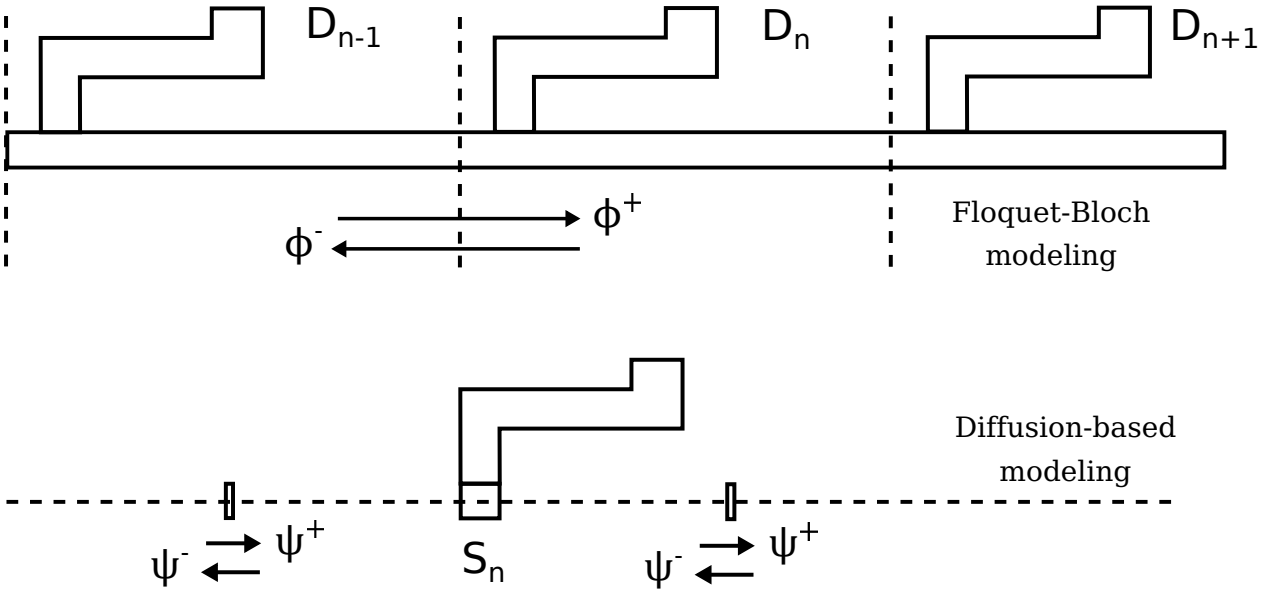

Figure 4: Concept of diffusion-based modeling.

3.2 Diffusion relations

Denoting $[\Psi^+, \Psi^-]$ the wave basis and $\mathbb{S}$ the condensed coupling element matrix, the local dynamic equilibrium can be rewritten using the state vectors expansion on the positive and negative-going wave amplitudes. Reorganizing the transmitted and reflected wave amplitudes and expressing in terms of the incident waves yields the following expression of the R and T coefficients:

$$\left\{ \begin{array}{c} R \\ T \end{array} \right\} = \left[\begin{array}{cc} A & B \\ C & D \end{array} \right]^{-1} \left\{ \begin{array}{c} \alpha \\ \beta \end{array} \right\} \tag{5}$$

where the matrix terms A, B, C and D are written:

$$A = \mathbb{D}_{RL}\Psi^{-}\Lambda + (\mathbb{D}_{RR} + \mathbb{S}_{LL})\Psi^{-} \tag{6}$$
$$B = \mathbb{S}_{LR}\Psi^{+} \tag{7}$$
$$C = \mathbb{S}_{RL}\Psi^{-} \tag{8}$$
$$D = (\mathbb{S}_{RR} + \mathbb{D}_{LL})\Psi^{+} + \mathbb{D}_{LR}\Psi^{+}\Lambda \tag{9}$$

The coefficients $\alpha_j = \mathbb{Q}_1(\lambda_j)\Psi_j^{+}$ and $\beta_j = \mathbb{Q}_2\Psi_j^{+}$ are the source terms associated with the incident wave of index j while $\mathbb{Q}_1$ and $\mathbb{Q}_2$ are the unit-cell dynamic projection matrices at the edges of the coupling element. Note that a modal synthesis can also be used to reduce the condensation effort on matrix $\mathbb{S}$. A major advantage however is that the wave basis remains unchanged and resonators' designs can be investigated without recomputing wave solutions.

3.3 Reduced formulation

Considering a wave projection basis Θ, built using the Wave Finite Element method, from a reduced subset of Bloch waves [14] (interested reader can also refer to Ref. [15, 16, 17, 18, 19] for further developments on reduced WFEM). Reduced dynamic stiffness matrix is therefore denoted $\tilde{\mathbb{D}}$ and $\tilde{\Psi} = \Theta^T\Psi$ is the reduced state vector, the spectral problem can be rewritten as:

$$[\Theta^T\mathbb{D}_{RL}(\omega)\Theta\tilde{\Lambda}^{-1} + \Theta^T(\mathbb{D}_{RR}(\omega) + \mathbb{D}_{LL}(\omega))\Theta + \Theta^T\mathbb{D}_{LR}(\omega)\Theta\tilde{\Lambda}]\tilde{\Psi} = 0 \tag{10}$$

The solutions of Eq.10 can be used to rewrite the diffusion equation (Eq.5) as:

$$\begin{bmatrix} \Theta^T & 0 \\ 0 & \Theta^T \end{bmatrix}\begin{bmatrix} A & B \\ C & D \end{bmatrix}\begin{Bmatrix} R \\ T \end{Bmatrix} = \begin{bmatrix} \Theta^T & 0 \\ 0 & \Theta^T \end{bmatrix}\begin{Bmatrix} \alpha \\ \beta \end{Bmatrix} \tag{11}$$

which results in the following reduced scattering and source coefficients:

$$\tilde{A} = \tilde{\mathbb{D}}_{RL}\tilde{\Psi}^{-}\tilde{\Lambda} + (\tilde{\mathbb{D}}_{RR} + \Theta^T\mathbb{S}_{LL}\Theta)\Psi^{-} \tag{12}$$
$$\tilde{B} = \Theta^T\mathbb{S}_{LR}\Theta\tilde{\Psi}^{+} \tag{13}$$
$$\tilde{C} = \Theta^T\mathbb{S}_{RL}\Theta\tilde{\Psi}^{-} \tag{14}$$
$$\tilde{D} = (\Theta^T\mathbb{S}_{RR}\Theta + \mathbb{D}_{LL})\tilde{\Psi}^{+} + \mathbb{D}_{LR}\tilde{\Psi}^{+}\tilde{\Lambda} \tag{15}$$

and

$$\tilde{\alpha} = \Theta^T\alpha\Theta \tag{16}$$
$$\tilde{\beta} = \Theta^T\beta\Theta \tag{17}$$

However, note that the coupling matrix is projected on the reduced wave basis: $\Theta^T\mathbb{S}_{ab}\Theta$. This operation may produce inaccuracies for evanescent wave diffusion properties, if the junction between the waveguide and the coupling part exhibit strong mismatch. This assumption is tested in the application example below.

4 Numerical validations

4.1 Validation of the ROM procedure

State vector projection on a reduced set of Bloch waves is highly effective to describe the propagation of free waves. However, the junction between the waveguide section and the coupling singularity may not be approximated correctly by the proposed state vector projection. Let us consider two coupling elements: model

(a) contains only the resonator with a small waveguide junction, while model (b) includes a large section of the waveguide whose dimension is the initial periodic unit-cell length. Model (b) is therefore expected to allow positive-going highly evanescent waves to decay along the coupling element, thus increasing the Bloch projection accuracy and the junction with the waveguide model.

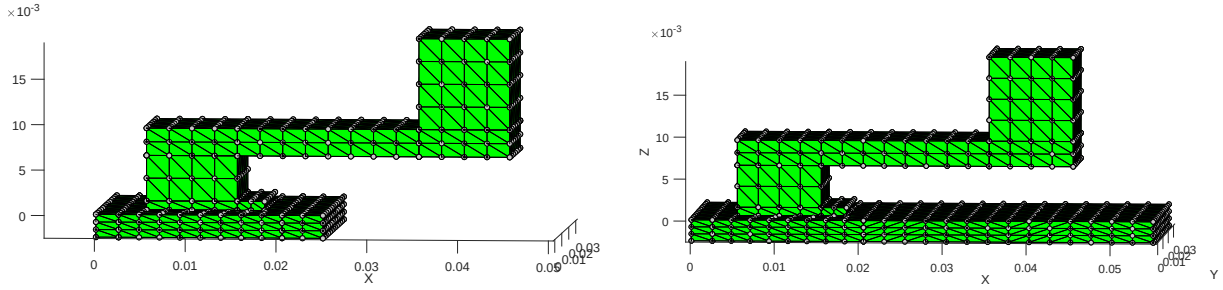

Figure 5: Two types of coupling element models. (a) Small coupling element and (b) Large coupling element (unit-cell standard length).

Diffusion coefficients are compared with the full solution. First we observe that dashed and continuous lines are close together. It means that the produced error is mainly due to the Component Mode Synthesis (CMS) reduction achieved on the coupling element. Inside the bandgap, the reduction scheme increases the initial CMS error. It can be explained since the internal resonance of the tuned mass damper produces near-field components (evanescent waves) that are not well described by the reduced wave basis. On the other hand, the short coupling (a) element appears less sensitive to the reduction than model (b), outside the bandgap. This can result from the fact that a higher number of modes are needed in model (b) to describe the inner dynamics of cell, compared with model (a).

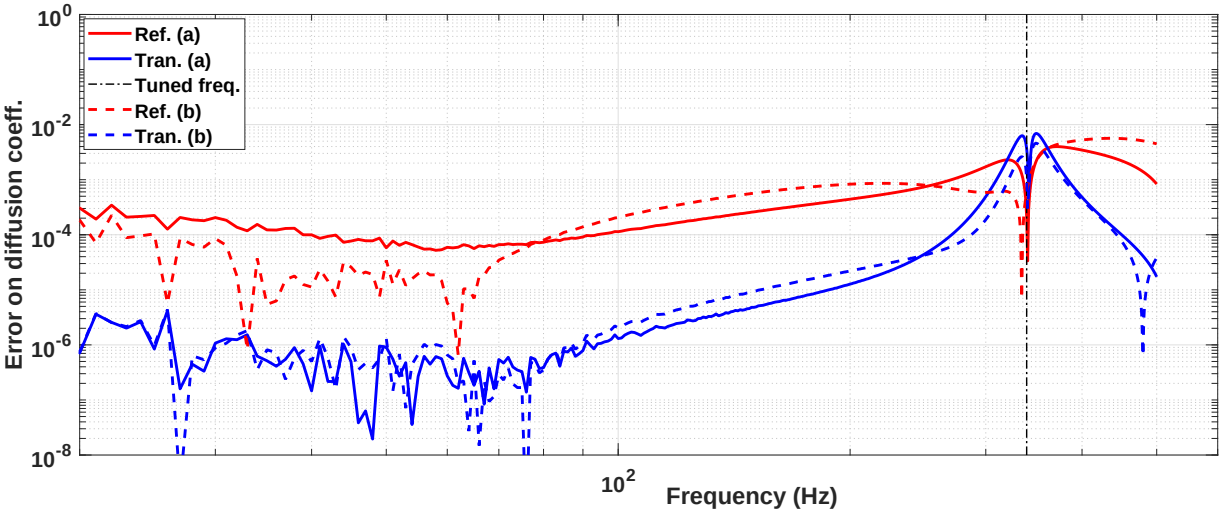

Figure 6: Error produced by the projection using different coupling element configurations.

It can be concluded that the projection of the coupling element on a reduced wave basis does not affect significantly the computed diffusion coefficients' accuracy in the considered example. In terms of CPU, the state vector reduction provides an overall reduction factor between 20× and 30×, depending on the requested accuracy.

4.2 Bloch vs. Diffusion information

The reflection and transmission coefficients are represented in Fig.7 for the model studied in Sec.2. Since the resonator is damped, dissipation occurs at resonance. Diffused wave coefficient is derived from energy balance and indicates the residual waves components:

- Transmission into propagating wavetypes (i.e. positive conversion)
- Transmission into evanescent waves (i.e. positive diffusion)
- Dissipation in the coupling element (i.e. absorption)
- Reflection into propagating wavetypes (i.e. negative conversion)
- Reflection into evanescent waves (i.e. negative diffusion)

In the context of the design of vibroacoustic metamaterials or locally resonant tuned mass dampers, the overall objective is to reduce (either by conversion or dissipation) the mechanical energy carried by the first-order flexural waves. In this regard, the residual component in Fig.7 contains both the specular (propagating) and diffuse (evanescent) scattering, as well as the wave absorption coefficient. It provides a good estimation of the resonator's performance.

The 'diffused' coefficient therefore corresponds to:

$$\{\text{diffused}\} = \{\text{positive diffusion}\} + \{\text{negative diffusion}\} + \{\text{absorption}\} \tag{18}$$

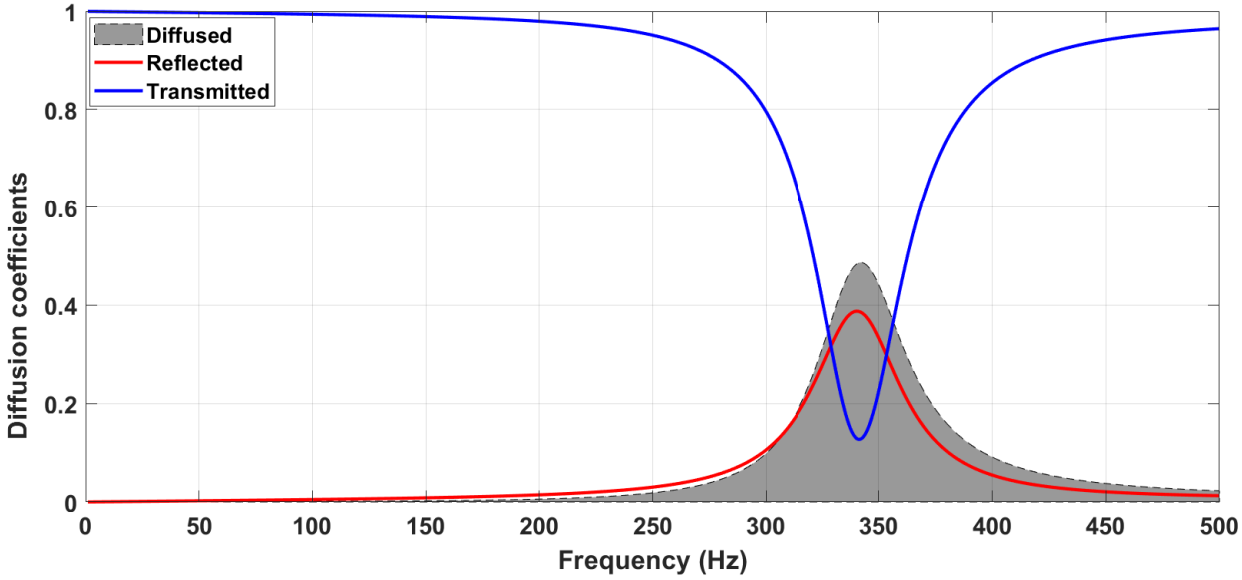

Figure 7: Diffused, reflected and transmitted waves through the resonator's coupling element.

As expected, the diffusion pic is located at the same frequency as the bandgap from Bloch analysis, and the transmission curve and propagation constants display similar patterns and are almost superposed. This time, an additional information is provided by the diffusion analysis: the Reflected and Diffused coefficients, where one can notice that the absorption is slightly higher than the reflection. In the following, the proposed diffusion model is used to investigate the influence of a resonator's design parameter on the absorption and reflection coefficients and on the overall dynamic response.

4.3 Vibration absorption performances and finite response

Additionally, for the selected waveguide, each new resonator can be analyzed without re-computing Bloch solutions, hence resulting in a considerable gains in terms of computational efforts (see Table 3). Indeed, the coupling element can be condensed (3 sec.) for the selected model, and diffusion analysis can be achieved in 7 sec. (0.2 sec. with the reduced wave basis) against 184 seconds for each design using the standard Bloch unit-cell analysis.

Modeling strategy	Unit-cell (Bloch)	Reduced diffusion
Added computation time per resonator's design (s)	**184**	**3.2**

Table 3: Computation times depending on the modelling choice and use of reduced WFEM formulation. All calculations are made with the same processor.

A parametric analysis is proposed in Fig.9 for the resonator's damping properties. The influence of the loss factor η on the distribution of transmitted and diffused waves is evaluated. Although the bandgap classically decreases in depth while its bandwidth increases with damping (see Reflection curve), the reflection is progressively replaced by the absorption starting from $\eta = 5\%$. Noteworthy, as the reflection decreases with damping, the absorption reaches a maximum then decreases, hence reducing the resonator's overall efficiency above $\eta \geq 10\%$. A compromise could therefore be reached for values of the damping, in order to achieve a low wave transmission while privileging absorption over reflection.

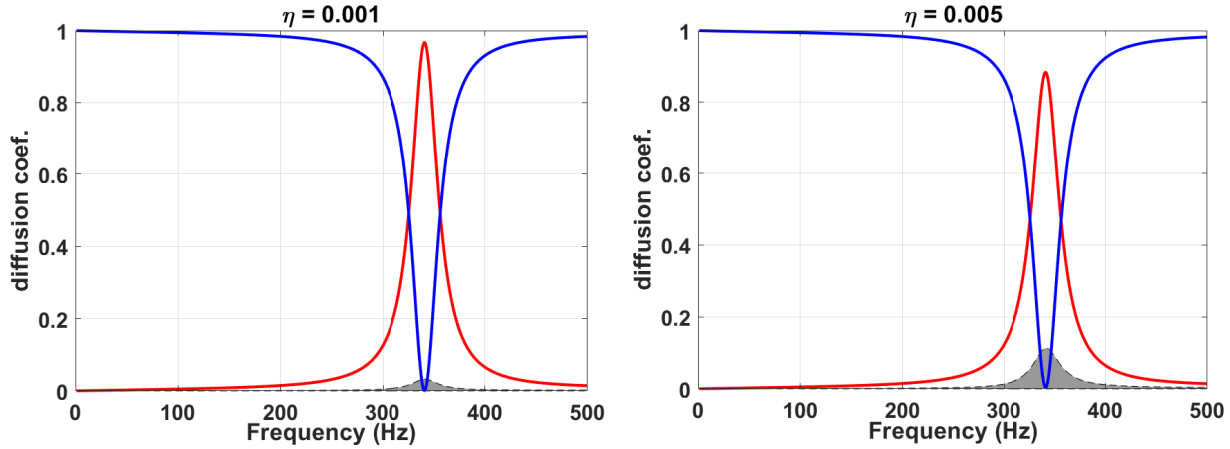

Figure 8: Influence of damping on the resonator's absorption and reflection coefficients.

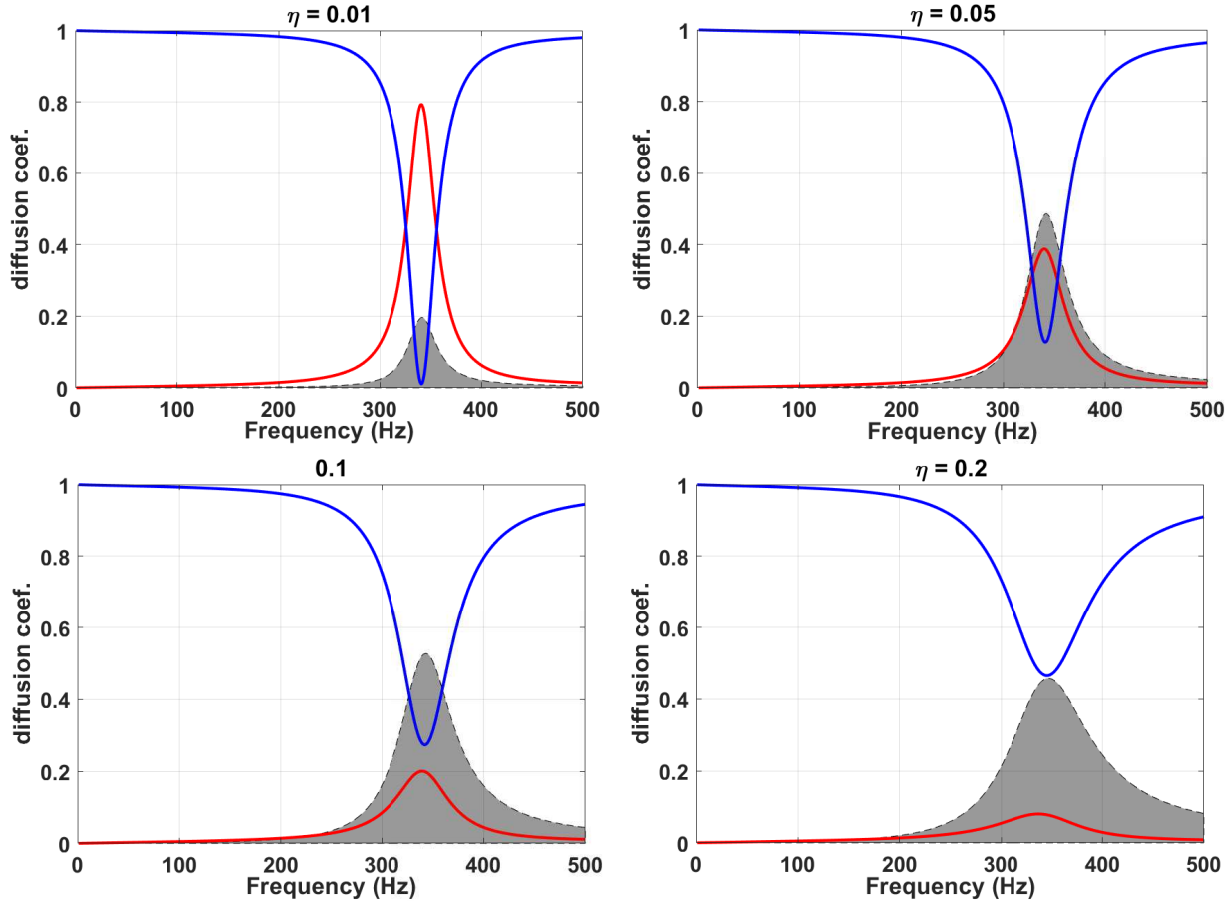

Figure 9: Influence of damping on the resonator's absoption and reflection coefficients.

The dynamic response for different damping values is shown in Fig.11. Note that an increased damping suppresses modes around the bandgap, thus it significantly increases the controlled bandwidth. Above these values damping becomes counter-productive within the bandgap region.

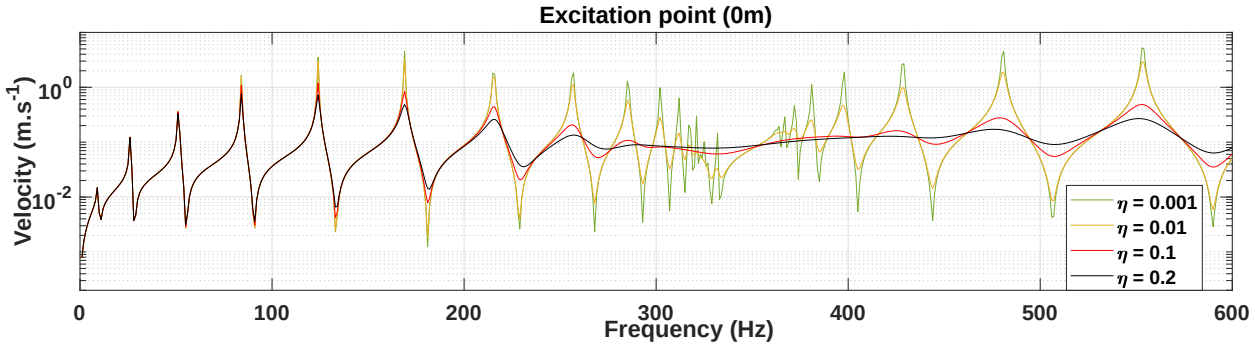

Figure 10: Influence of damping on the finite waveguide's dynamic response. Three posistions from excitation point (0 cm, 10 cm, 50 cm) and four values of the damping ($\eta = 0.001 - 0.2\%$)

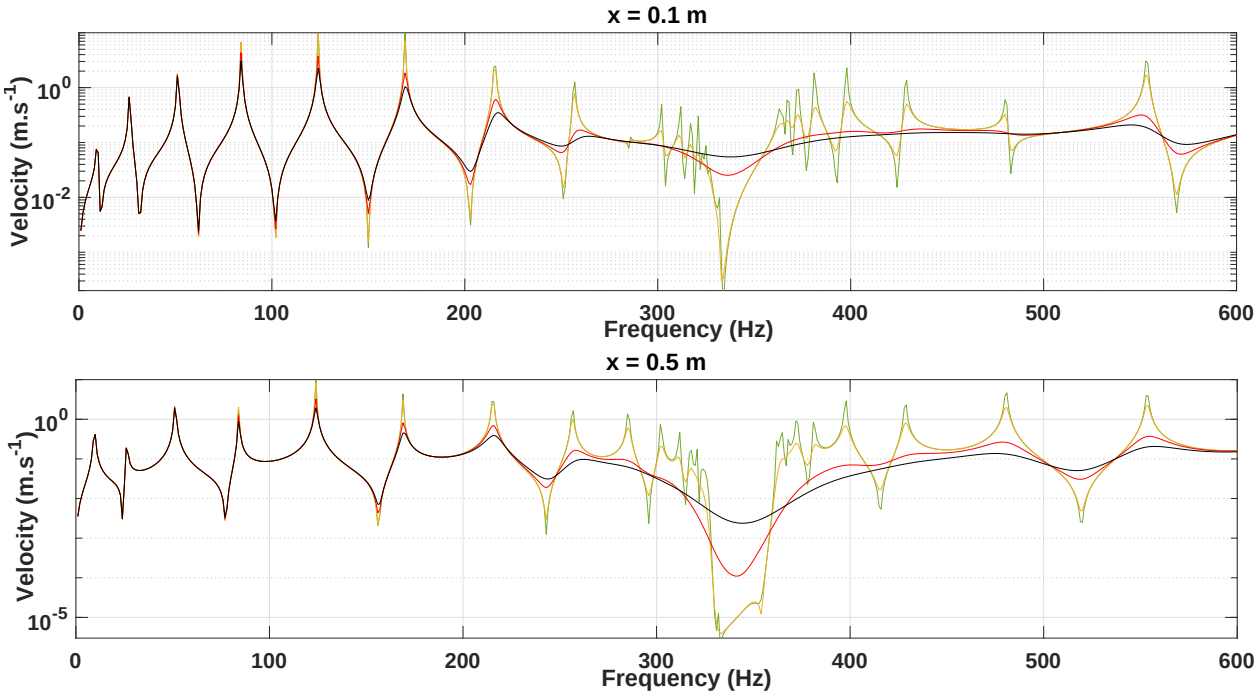

Figure 11: Influence of damping on the finite waveguide's dynamic response. Three posistions from excitation point (0 cm, 10 cm, 50 cm) and four values of the damping ($\eta = 0.001 - 0.2\%$)

5 Conclusions

In this paper an alternative diffusion-based methodology was used to study a locally resonant sub-structure and compared with Bloch diagram analyses. The method proved highly effective to predict wave reflection, transmission, and diffusion coefficients, including evanescent conversion and absorption. A reduced formulation based on Bloch wave expansion was proposed to reduce the computation effort so that the influence of resonators' damping properties could be investigated. It is emphasized that better damping models could be implemented, as the coupling dynamic stiffness matrix can involve viscoelastic materials or external loads. The proposed methodology provides additional information compared with Bloch analyses. It is hoped that the proposed method will prove efficient for the fast design optimization of Bragg or locally resonant metamaterials.

References

[1] Igusa, T., Xu, K. (1994). *Vibration control using multiple tuned mass dampers*. Journal of sound and vibration, 175(4), 491-503. (https://doi.org/10.1006/jsvi.1994.1341)

[2] Yamaguchi, H., Harnpornchai, N. (1993). *Fundamental characteristics of multiple tuned mass dampers for suppressing harmonically forced oscillations*. Earthquake engineering & structural dynamics, 22(1), 51-62. (https://doi.org/10.1002/eqe.4290220105)

[3] Xiao, Y., Wen, J., Wen, X. (2012). *Broadband locally resonant beams containing multiple periodic arrays of attached resonators*. Physics Letters A, 376(16), 1384-1390. (https://doi.org/10.1016/j.physleta.2012.02.059)

[4] Claeys, C., Deckers, E., Pluymers, B., Desmet, W. (2016). *A lightweight vibro-acoustic metamaterial demonstrator: Numerical and experimental investigation*. Mechanical Systems and Signal Processing, 70, 853-880. (https://doi.org/10.1016/j.ymssp.2015.08.029).

[5] Mencik, J. M., Ichchou, M. N. (2005). *Multi-mode propagation and diffusion in structures through finite elements*. European Journal of Mechanics-A/Solids, 24(5), 877-898. (https://doi.org/10.1016/j.euromechsol.2005.05.004)

[6] Mitrou, G., Ferguson, N., Renno, J. (2017). *Wave transmission through two-dimensional structures by the hybrid FE/WFE approach*. Journal of Sound and Vibration, 389, 484-501. (https://doi.org/10.1016/j.jsv.2016.09.032)

[7] Ben Souf, M.A., Kessentini, A., Bareille, O., Taktak, M., Ichchou, M. N., Haddar, M. (2017). *Acoustical scattering identification with local impedance through a spectral approach*. Comptes Rendus Mcanique, 345(5), 301-316. (https://doi.org/10.1016/j.crme.2017.03.006)

[8] Becht, P., Deckers, E., Claeys, C., Pluymers, B., Desmet, W. (2016). *Using the resonance behavior of finite pipes for defect detection based on the wave-scattering*. Proceedings of ISMA 2016 - International Conference on Noise and Vibration Engineering, 2014, p. 1147-1161. (http://past.isma-isaac.be/downloads/isma2016/papers/isma2016_0775.pdf)

[9] Errico, F., Ichchou, M., De Rosa, S., Bareille, O., Franco, F. (2018). *A WFE and hybrid FE/WFE technique for the forced response of stiffened cylinders*. Advances in Aircraft and Spacecraft Science, 5(1), 1-19. (https://doi.org/10.12989/aas.2018.5.1.001)

[10] Errico, F., Ichchou, M., De Rosa, S., Bareille, O., Franco, F. (2018). *The modelling of the flow-induced vibrations of periodic flat and axial-symmetric structures with a wave-based method*. Journal of Sound and Vibration, 424, 32-47. (https://doi.org/10.1016/j.jsv.2018.03.012)

[11] Gravenkamp, H. (2018). *Efficient simulation of elastic guided waves interacting with notches, adhesive joints, delaminations and inclined edges in plate structures*. Ultrasonics, 82, 101-113. (https://doi.org/10.1016/j.ultras.2017.07.019)

[12] Droz, C., Bareille, O., Laine, J.P., Ichchou, M. (2018). *Wave-based SHM of sandwich structures using cross-sectional waves*, Structural Control and Health Monitoring, vol. 25(2), e2085. (https://doi.org/10.1002/stc.2085)

[13] Lossouarn, B., Aucejo, M., De, J. F. (2018). *Electromechanical wave finite element method for interconnected piezoelectric waveguides*. Computers & Structures, 199, 46-56. (https://doi.org/10.1016/j.compstruc.2018.01.009).

[14] C. Droz, J. P. Lainé, M. Ichchou, G. Inquiété. (2014). *A reduced formulation for the free-wave propagation analysis in composite structures*, Composite Structures, vol. 113, p. 134-144. (https://doi.org/10.1016/j.compstruct.2014.03.017)

[15] C. Droz, M. Ichchou, J. P. Lainé. (2014). *Numerical prediction of dispersion characteristics for high-order waves in composite waveguides*, Proceedings of ISMA 2014 - International Conference on Noise and Vibration Engineering, 2014, p. 4203–4216. (http://past.isma-isaac.be/downloads/isma2014/papers/isma2014_0043.pdf)

[16] Zhou, C.W., Laine, J.P., Ichchou, M., Zine, A.M. (2015). *Wave finite element method based on reduced model for one-dimensional periodic structures*. International Journal of Applied Mechanics, 7(02), 1550018. (https://doi.org/10.1142/S1758825115500180)

[17] Droz, C., Zhou, C., Ichchou, M., Lainé , J. P. (2016). *A hybrid wave-mode formulation for the vibro-acoustic analysis of 2D periodic structures*, Journal of Sound and Vibration, Vol. 363, p. 285-302. (https://dx.doi.org/10.1016/j.jsv.2015.11.003)

[18] Fan, Y. , Zhou, C.W., Laine, J.P., Ichchou, M., Li, L. (2018). *Model reduction schemes for the wave and finite element method using the free modes of a unit cell*. Computers & Structures, 197, 42-57. (https://doi.org/10.1016/j.compstruc.2017.11.015)

[19] Boukadia, R., Droz, C., Ichchou, M., Desmet, W. (2018). *A Bloch wave reduction scheme for ultrafast band diagram and dynamic response computation in periodic structures*, Finite Elements in Analysis and Design, vol. 148, p.1-12. (https://doi.org/10.1016/j.finel.2018.05.007)